Published in final edited form as:
J Biomed Mater Res B Appl Biomater. 2013 August ; 101(6): . doi:10.1002/jbm.b.32914.

Toward single-walled carbon nanotube–gadolinium complex as advanced MRI contrast agents: pharmacodynamics and global genomic response in small animals

Pramod K. Avti[1], **Yahfi Talukdar**[1], **Matvey V. Sirotkin**[2], **Kenneth R. Shroyer**[3], and **Balaji Sitharaman**[1]

[1]Department of Biomedical Engineering, Stony Brook University, Stony Brook, New York 11794-5281

[2]Department of Mechanical Engineering, Stony Brook University, Stony Brook, New York 11794-3000

[3]Department of Pathology, Stony Brook University, Stony Brook, New York 11794-8691

Abstract

Gadolinium nanoparticle-catalyzed single-walled carbon nanotubes (Gd-SWCNTs) have recently shown potential *in vitro* as high-performance T_1 magnetic resonance imaging (MRI) contrast agents (CAs). Their preclinical safety assessment at nontoxic dosages is essential for MRI applications. Herein, the *in vivo* (in rats) pharmacodynamics of Gd-SWCNTs (water solubilized with the amphiphilic polymer PEG-DSPE) at the organ, tissue, molecular, and genetic level is reported. Gd-SWCNT, commercially available iron catalyzed SWCNTs (Fe-SWCNTs, control 1) and PEG-DSPE (control 2) solutions were intravenously injected at a potential nontoxic therapeutic dose (0.5 mg/kg body weight, single bolus). Post-injection, bright-field optical microscopy showed their macroscale distribution in lung, liver, kidney, brain, and spleen up to 5 days. Raman and transmission electron microscopy (TEM) showed their presence at the nanoscale within hepatocytes. Their effects on the host organ tissue, molecular, and genetic level were analyzed after 1, 5, 10, 20, and 30 days by histology, biomolecular [lipid peroxidation, plasma tumor necrosis factor TNF-α assay, microarrays] assays. The results indicate that Gd-SWCNTs neither cause any inflammation, nor damage to the above organs, nor any significant change in the lipid peroxidation or plasma proinflammatory cytokine (TNF-α) levels for all the groups at all time points. Global gene expression profile of liver (main organ for the metabolism) after day 1 treatment with Gd-SWCNTs shows that the gene regulation is directed toward maintaining normal homeostasis. The results taken together indicate that PEG-DSPE water-solubilized Gd-SWCNTs at potentially nontoxic dosages have pharmacodynamics similar to other commercially available Fe-SWCNTs and are suitable for future preclinical development as *in vivo* MRI CAs.

Keywords

animal model; biomaterials availability; histology; nanomedicine; molecular imaging

Correspondence to: B. Sitharaman; balaji.sitharaman@stonybrook.edu.

Additional Supporting Information may be found in the online version of this article.

INTRODUCTION

Over the past two decades, contrast-enhanced magnetic resonance imaging (MRI) has become a powerful and indispensable tool for noninvasive preclinical cellular and molecular imaging and clinical diagnosis.[1,2] MRI procedures use contrast agents (CAs) to improve sensitivity and diagnostic confidence. Gadolinium ion (Gd^{3+}) small molecule chelate complexes shorten the T_1 or spin-lattice relaxation time of the water protons and are most widely used T_1 MRI CAs used in clinic.[3,4] These Gd^{3+} molecule chelate complexes are adequate as first-pass extracellular fluid MRI CAs. However, they can enhance the contrast down to micromolar (μM) concentrations[5] and are unsuitable for advanced cellular and molecular MRI application, which requires MRI CAs to be efficacious in the nanomolar to picomolar concentrations.[6] Thus, the chemistry and design of Gd^{3+}-based advanced MRI CAs remains an active area of research with a major focus on improving/increasing their relaxivity (an important measure of efficacy), which would lower their detection limit by MRI.

Recent progress in Gd^{3+} carbon nanotube complexes has allowed the development of high-relaxivity T_1 MRI CAs.[7–11] *In vitro* and *in vivo* (in rodents) efficacy studies show that these MRI CAs show potential for MRI-based molecular and cellular imaging.[10–13] *In vitro* studies have assessed the cytotoxicity of these MRI CAs and identified dosages at which they show no cytotoxic effects.[10,11] However, till date, there have been no *in vivo* reports that have assessed the safety of these MRI CAs. *In vivo* pharmacological assessment at nontoxic doses is especially critical for Gd^{3+}-carbon nanotube complexes because of the recent concerns on the clinical use of the Gd^{3+}-based clinical MRI CA, which in some patients with severe renal disease or after liver transplant generated nephrogenic systemic fibrosis (NSF),[14] leading to Food and Drug Administration restrictions.[15] In addition, there is an emerging consensus that the *in vivo* toxicity of single-walled carbon nanotubes (SWCNTs) is not only dose- and time-dependent but also dependents on a number of other factors such as size of SWCNTs, dispersing agents to water solubilize the hydrophobic nanotubes, the catalysts used in their preparation, and their method of administration.[16] Therefore, pharmacology of every new SWCNT-based complex must be assessed individually as a different compound.

We have recently synthesized, using a “bottom-up” chemical approach, a novel Gd-SWCNT complex that shows potential as a multimodal MR-optical imaging nanoprobe.[17–19] Our synthesis method uses lanthanide nanoparticles (average size ~1.8 nm) as catalysts to grow SWCNTs (hereafter referred as Gd-SWCNTs; average diameter 2.05 nm, length 500 nm to 1.5 μm)[17] with the lanthanide nanoparticles embedded into and located at one end of the SWCNT.[18] The Gd-SWCNTs are paramagnetic, and at clinically relevant 1.5 T magnetic field, show r_1 relaxivity (an important measure of efficacy) values of 126 $mM^{-1}S^{-1}$; 25-fold greater than the current, clinically used Gd^{3+}-based CA Magnevist (4.5 $mM^{-1}S^{-1}$).[19] Recent *in vitro* studies have also identified nontoxic dosages of water-solubilized Gd-SWCNTs that do not affect cellular anatomy or function.[20] These studies also demonstrate that the Gd-SWCNTs are suitable as magnetic labels for cellular MRI. In this article, we report the *in vivo* (in rats) pharmacodynamics of water-soluble Gd-SWCNTs at the organ/ tissue, molecular, and genomic level at a potentially nontoxic dosage.

MATERIALS AND METHODS

Synthesis and functionalization of the Gd-SWCNTS

The Gd-SWCNTs were synthesized by chemical vapor deposition (CVD; Easy Tube 2000, First Nano, Ronkonkoma, NY) as described elsewhere.[17] The hydrophobic Gd-SWCNTs were water-solubilized by dispersing 1 mg of Gd-SWCNTs in 1 mL of saline solution

containing 0.2 m*M* of the amphiphilic polymer *N*-(Carbonyl-methoxypolyethyleneglycol 2000)-1,2-distearoylsn-glycero-3-phosphoethanolamine (PEG-DSPE) (NOF Corporation, USA) by probe sonication (Cole Palmer, Vernon Hills, Illinois) at 300 W for 10 min followed by centrifugation at 7000*g*.[21] The supernatant was used for the *in vivo* studies. The nanotube concentration was determined by optical absorption spectroscopy.[18] Commercially available purified SWCNTs (Unidym, CA) synthesized using iron as a catalyst (Fe-SWCNTs) was used as control 1 and dispersed in PEG-DSPE as described above.

Animal experiments

Animal experiments were performed in accordance with the approved protocol by Stony Brook University's Institutional Animal Care and Use Committee. Male Wistar rats (6 weeks old) obtained from Charles River Laboratories (Wilmington, MA) were individually housed, allowed free access to water, fed standard rat chow pellets, and kept on a 12-h light–dark cycle. The weight of each animal was recorded weekly. Before the experiments were conducted, the animals were acclimatized for a week at the above conditions. The animals were divided into three groups (five rats per group): (a) Gd-SWCNT—experimental group that received an intravenous (IV) injection of Gd-SWCNTs dispersed in saline solution containing 0.2 m*M* PEG-DSPE, (b) Fe-SWCNT—control group (control 1) that was received an IV injection of Fe-SWCNTs dispersed in saline solution containing 0.2 m*M* PEG-DSPE, and (c) PEG-DSPE—control group (control 2) that received an IV dose of saline solution containing 0.2 m*M* PEG-DSPE. For each group, a single IV dose (0.5 mg/kg body weight) was injected via the tail vein. The animals from the above three groups were euthanized by CO_2 inhalation at 1, 5, 10, 20, or 30 days post-treatment. Blood was collected, and the animals were perfused with ice-cold solution (0.15*M* KCl, 2 m*M* EDTA, pH 7.4). Liver, lungs, kidneys, brain, and spleen were excised and perfused with ice-cold perfusion solution (0.15*M* KCl, 2 m*M* EDTA, pH 7.4).

Preparation of the histological specimens

The liver, lung, kidney, brain, and spleen were fixed in 10% buffered formalin (pH 7.2), dehydrated through a series of ethanol solutions, and embedded in paraffin. Five-micron thick sections were cut and stained with hematoxylin-eosin (H&E) for histological analysis. Bright-field optical microscopy images of the stained tissues were obtained using aBX-51 Olympus microscope (Hamburg, Germany) attached with a charge-couple device (CCD) camera. The same microscope was used for the histopathological analysis.

TEM

Various organ tissues were perfused and fixed using solution A (2% paraformaldehyde and 2.5% glutaraldehyde in 0.1*M* phosphate saline, pH 7.4). The fixed specimens were placed in 2% osmium tetroxide in 0.1*M* PBS solution, dehydrated in a graded series of ethyl alcohol, and embedded in EPON resin. Areas of interest were blocked, cut into ~75 nm ultrathin sections with a Reichert-Jung Ultracut ultramicrotome and placed on formvar-coated copper slot grids. The sections were then viewed with a FEI Tecnai BioTwinG^2 transmission electron microscope at 80 kV. Digital images were acquired with an AMT XR-60 CCD digital camera system.

Raman microscopy

The paraffin-embedded liver tissues, cut into 5-μm thick sections, were analyzed for the presence of Gd-SWCNT using DXR Raman Microscope (ThermoFisher Scientific, Milan, Italy). The tissue sections were subjected to dispersive Raman measurements using an excitation laser at 780 nm using a 50× objective. The Raman spectra were obtained for a number of points on the tissue section. Point-by-point Raman spectra were obtained over

selected areas corresponding to the region of Gd-SWCNT distribution in the tissue and mapped. The area maps constructed using the G-band intensity of the Gd-SWCNTs was overlaid over the optical images for their localization and analysis.

Immunohistochemistry

Tissues were fixed in neutral-buffered formalin, paraffin-embedded, and sectioned at 5 μm. After deparaffinization, antigen retrieval was performed in citrate buffer [20 mmol/L (pH 6.0)] at 120°C for 10 min in a decloaking chamber. Before incubation with the antibody, the sections were treated with an avidin–biotin endogenous biotin removal kit (Vector) to block background staining from endogenous biotin. Sections were incubated overnight with rabbit polyclonal antimyeloperoxidase antibody (Abcam) diluted 1:125, followed by detection with an avidin–biotin-based system (Vectastain ABC Elite) and development with 3,3′-diaminobenzidine (Dako). After hematoxylin counterstaining, sections were imaged using bright-field microscopy. Negative controls were performed by substituting the primary antibody solution with Tris-buffered saline–tween 20 (TBS-T) buffer. The myeloperoxidase (MPO) expression for each group was scored by counting, and averaging the MPO stained neutrophils in 10 different field views at 40× magnification.

Lipid peroxidation (LPx) assay

Organs harvested from the rats were homogenized in 1:3 w/v of Tris-HCl buffer (50 m*M*, pH 7.4), and the homogenates centrifuged at 10,000*g* at 4°C for 30 min. The supernatant was used for the lipid peroxidation analysis. Blood was centrifuged at 1000 rpm for 15 min, and the supernatant containing the plasma was collected. Lipid peroxidation in the plasma and tissues were analyzed according to a protocol developed by Hendriks and Assmann.[22] For the lipid peroxidation assay, 100 μL of the tissue homogenate or plasma was added to 0.9 mL PBS in a glass vial. A total of 1 mL of 20% acetic acid (pH 2.5) and 1 mL of 0.08% thiobarbituric acid was added, and the glass vial was heated to 95°C for 1 h. The vial was then cooled, HCl (25 μL, 5*N*) followed by 3 mL butanol was added. The vials were agitated and allowed to separate into layers. The butanol layer was used for quantifying the thiobarbituric acid reactive substances formed by reaction of malondialdehydes (MDA) and thiobarbituric acid. A fluorometer at 530/25 excitation and 580/50 emission was used (Cytofluor Series 4000, PerSeptive Biosystems, MA). MDA standards (1,1,3,3-tetramethoxypropane) of 1–100 ng/mL were used for preparing the standard curve.

Plasma TNF-α assay

To determine the plasma tumor necrosis factor-α (TNF- α) levels, enzyme-linked immunosorbent assay was performed by using commercial kits that are selective for rat TNF-α (R&D Systems, USA) following the manufacturer instructions. The absorbance was measured on a microplate reader at 450 nm wavelength (Varioskan Flash, Thermo Electron, Finland), and the TNF-α concentration in the samples was calculated from a standard curve.

Whole genome expression analysis

Liver samples of three rats of similar weight from each of the three groups (one experimental and two control groups) were harvested 1 day postinjection. Gene expression profiles of the tissues from these three groups were compared using Affymetrix Rat Genome 230 2.0 microarrays (Affymetrix, CA). Total RNA was isolated using TRIzol reagent (Invitrogen, CA) according to the manufacturer protocols, and RNeasy Mini Kit (Qiagen, CA) was used to purify the RNA. The RNA was stored at −80°C. The RNA was then submitted to the Genomics Core facility Lab (Stony Brook University, NY). The RNA quality was analyzed using an Agilent 2100 Bioanalyzer. The cDNA generated was labeled using one-cycle target labeling method. cDNA generated from each sample was hybridized

to a single array according to standard Affymetrix protocols. A total of nine microarrays were used—three arrays for each harvested liver sample.

Statistics

The data for tissue and plasma lipid peroxidation and plasma TNF-α are presented as mean ± standard deviation. Statistical significance was analyzed by ANOVA using IBM Statistical Project for Services Solution (SPSS) software. Comparisons with p value less than 0.05 were considered significant. For the microarray studies, the Affymetrix raw image data were normalized using RMA (robust multiarray analysis) algorithm of GenPattern Software (Broad Institute, MIT and Harvard). Differential expression analysis was performed by two-tailed t test. Probes with $p < 0.05$ and at least twofold change were selected. Annotations were from Affymetrix NetAffx resource. Differentially expressed genes were classified based on their known biological functions using the Database for Annotation, Visualization, and Integrated Discovery (DAVID) software.

RESULTS AND DISCUSSION

The studies reported in this article were performed to address the following two questions: (1) What effects do water-soluble Gd-SWCNTs have at the organ/ tissue, molecular, and genomic level at a potentially nontoxic dosage? (2) Are these effects different from the widely used water-soluble Fe-SWCNTs? The studies were part of a larger goal of developing these nanoparticles as MRI CAs. The dosage of 0.5 mg/kg was chosen from previous *in vitro* studies on the Gd-SWCNTs that show that these nanoparticles at 10 μg/mL concentrations do not have any effects on cell anatomy or function.[20] This dosage is 10 times lower than dosages where Fe-SWCNTs elicit a toxic response *in vivo.*[16] The hydrophobic nanotubes were noncovalently functionalized with PEG-DSPE, because previous reports on Fe-SWCNTs show that it imparts good water solubility to the hydrophobic nanotubes and to form stable suspensions in buffers or whole blood serum without any SWCNT aggregation.[16,21,23] Furthermore, for potential molecular MRI applications, PEG-DSPE allows functionalization of ligands for targeting molecules, cells, or tissues. In addition, PEG repels nonspecific interaction, is antibiofouling, has been shown to prolong blood circulation half-life (5 h), reduce reticuloendothelial (RES) uptake, and accelerate excretion.[23] These are essential features for potential advanced cellular and molecular MRI applications. The studies were performed up to 30 days, because for certain applications such as contrast-enhanced tracking of stem cells, the nanoparticles could remain *in vivo* for at least as long as 30 days.

The general health and behavior of the animals was monitored for all the animals used in this study. There was no significant change either in the body weight or the organ weight (lung, brain, kidney, liver, or spleen) between the Gd-SWCNTs, Fe-SWCNTs (control 1), and PEG-DSPE (control 2) groups at all time points. In addition, there were no behavioral changes, such as hunched posture, huddling, decreased appetite, increased or labored respiration, which indicates pain and discomfort, in any animals during the entire study. The Gd-SWCNT and the controls could not be detected beyond day 5 in the histological specimens of any of the organs, and results at day 1 and day 5 were similar. Thus, histology and TEM results of only day 1 are presented and discussed. Histology and TEM results for day 5 have been included in the Supporting Information section.

Organ/tissue response

Figure 1 shows representative images of histological specimens in the main organs; lungs, brain, kidney, liver, and spleen for PEG-DSPE [Figure 1(a–e)], Fe-SWCNT [Figure 1(f–j)], and the Gd-SWCNTs [Figure 1(k–o)] at day 1. All the organs for the three groups show

normal tissue morphology and no structural changes. The Gd-SWCNTs accumulate as aggregates (red arrows) in these organs. Similar sized aggregates were also found in the organs of animals treated with Fe-SWCNTs. The Gd-SWCNTs accumulate in the alveoli and epithelial linings of the lungs [Figure 1(k)], cerebral cortex of the brain [Figure 1(l)], glomerulus and proximal/distal tubules of the kidney [Figure 1(m)], hepatocytes of the liver near the hepatic portal vein [HPV; Figure 1(n)], and red pulp of spleen [Figure 1(o)]. TEM (Supporting Information Figure S2) and Raman microscopy (Supporting Information Figure S3) performed on liver tissue histology specimens indicate that the Gd-SWCNTs also accumulate within hepatocytes. The distribution and localization results taken together suggest that the Gd-SWCNTs are present in the extracellular matrix and inside the cells in the various organs.

Histopathological analyses were performed on tissue sections of lungs, brain, liver, kidney, and spleen at all the time points (day 1–30) for the Gd-SWCNTs and control groups. In general, the organs did not show any signs of major inflammation or damage to the tissue architecture. In addition, for all the organs, the histological specimens of Gd-SWCNTs were similar to those of Fe-SWCNTs and PEG-DSPE. At day 1, the lung histological specimens of the Gd-SWCNTs [Figure 1(k)] showed few inflammatory cells (macrophages), although not surrounding the Gd-SWCNTs aggregates. Because alveolar macrophages play a pivotal role in phagocytosis, immunological homeostasis, and host defense and might be key regulators in excreting the Gd-SWCNTs from the lungs. It is known that lungs secrete pulmonary surfactants. These surfactants maybe getting adsorbed and coated on the surface of Gd-SWCNTs, and thus, mitigate any inflammatory response because of their presence. The brain histological specimens of Gd-SWCNTs [Figure 1(l)] showed nanotube aggregates in the cerebral cortex. Intensely stained neurons were observed surrounding the Gd-SWCNTs. Inflammatory cells were not observed around the Gd-SWCNTs or the neurons surrounding the nanotube aggregates. Presence of Gd-SWCNTs in the cerebral cortex did not alter the tissue architecture. The kidney histological specimen of the Gd-SWCNTs [Figure 1(m)] showed no tissue damage or inflammatory response. Most of the Gd-SWCNTs were aggregated in the glomerulus, proximal, and distal tubules of the kidney. The glomerulus, proximal, and distal tubules form the filtration and excretion part of the kidney. Presence of the Gd-SWCNTs in these structures suggests that the Gd-SWCNTs are being transported by the systemic circulation and accumulate in the kidney for excretion. The Gd-SWCNTs [Figure 1(n)] liver tissue histological specimens also showed no tissue damage or inflammatory response. Gd-SWCNTs are accumulated in the hepatocytes of the liver much toward or close to the HPV. The liver receives 75% of blood supply through HPV, which transports blood from gastrointestinal tract and spleen and provides nutrients to liver. Presence of Gd-SWCNTs around the HPV shows that majority of hepatocytes in close proximity of the HPV are active and not damaged. The presence of Gd-SWCNTs in the spleen [Figure 1(o)] did not alter the histology of the spleen. The spleen is characterized by rich red pulp containing lot of red blood cells (RBCs) and immune cells, major site for RBC replenishment, making it difficult to identify the presence of the Gd-SWCNTs in the intensely stained cells.

Immunohistochemical analysis was also performed on the histological specimens of the lung, kidney, liver, and spleen treated with the Gd-SWCNTs and Fe-SWCNTs. The analysis involved staining the histological specimens with antibodies that detect the presence of the MPO enzyme, and thus, proinflammatory neutrophils cells. This staining was followed by a semiquantitative scoring method, wherein, for each group, the average number of MPO stained neutrophils (excluding the plasma cells and cells in the blood vessel) were obtained. MPO is a key enzyme activated by proinflammatory neutrophils that catalyzes the formation of reactive oxygen species.[24] Figure 2 shows representative bright-field optical images of the immunostained specimens, and Table I lists the average number of MPO stained

neutrophils for each organ per group. Figure 2 clearly shows that the small aggregates of Gd-SWCNTs did not attract any neutrophils. The average number of MPO-stained neutrophils for the Gd-SWCNTs and Fe-SWCNT (control 1) were 10–16 in the lung, 17–19 in the liver, and ≤2 in the kidney, liver, and brain. These values are typical for normal histological sections of these organs. Usually chemical-induced inflammation results in ≥20 average number of inflammatory cells.[25] The absence of neutrophils around the Gd-SWCNTs, and Fe-SWCNT accumulation site and low average number of inflammatory cells confirm that the proinflammatory neutrophils are not activated due to the presence of the Gd-SWCNTs, or Fe-SWCNTs, and corroborates the results of the histopathological analysis. The results show no noticeable evidence of SWCNT metabolism as reported in recent articles.[26,27] This lack of metabolic activity may be due to the noncovalent coating of the Gd-SWCNTs with PEG-DSPE and other proteins or lipids *in vivo* that may slowdown the metabolism of these nanoparticles.[27,28]

The above histopathological and immunohistochemical results are not in agreement with previous reports on Fe-SWCNTs, wherein their direct inhalation into the lungs through trachea induced granuloma.[29,30] The results also differ from another recent study with Fe-SWCNTs covalently functionalized with carboxylic acid groups and injected intraperitoneally at the same dosage (0.5 mg/kg).[31] That study showed karyomegaly (condensed nuclei) of hepatocytes and partial central vein damage leading to liver damage. However, our study cannot be directly compared either with above studies because the SWCNT aspect ratios, water-soluble functional groups, and the mode of injection were different. The accumulation of the Gd-SWCNTs and Fe-SWCNTs in the brain is interesting and suggests that at least a small fraction of the injected nanotubes cross the blood–brain barrier. Although the uptake and effects of functionalized Fe-SWCNTs after direct intracranial administration has been evaluated,[31,32] other reports suggest that direct IV injection of the nanotubes does not penetrate the normal brain tissue.[33,34] The presence of the Gd-SWCNTs and Fe-SWCNTs in the kidney, liver, and spleen suggests that they are cleared from the body by both the major routes; renal filtration (accumulation in kidney, and excretion through urine bladder) and hepatobiliary excretion (accumulation in the RES of liver and spleen and excretion thorough the bile). Studies have shown that the surfactants that water-solubilizing the nanotubes play an important role in their elimination from the body. Fe-SWCNTs dispersed in various surfactants (Tween-80, pluronic F108, and PEG-DSPE) are cleared from the systemic circulation by macrophages within few hours of the treatment or accumulate in RES of liver and spleen up to few months.[21,23,35–37] However, it still remains to be determined how the aggregated Gd-SWCNT or Fe-SWCNTs over time are eliminated from the liver or spleen. Studies suggest that the SWCNTs are oxidatively metabolized *in vivo* by a neutrophil enzyme MPO even though the extent of metabolism is slow.[27] Thus, the nanotubes maybe excreted in both their intact (absence of reactive intermediates) and metabolized state.

Molecular response

Figure 3 shows the lipid peroxidation levels in the liver, kidneys, spleen, lungs, and blood of rats treated with PEG-DSPE, Fe-SWCNT, or Gd-SWCNT solutions at four time points (day 1, 10, 20, and 30). The results show that, compared with PEG-DSPE, rats treated with Fe-SWCNTs and Gd-SWCNTs have higher lipid peroxide (LPx) levels in various organs. But, higher levels of LPx in Fe-SWCNT and Gd-SWCNT groups compared with PEG-DSPE groups were not statistically significant at all the time points. In the liver [Figure 3(a)], Fe-SWCNTs and Gd-SWCNTs show significant increase in LPx compared with PEG-DSPE only at day 1. The liver LPx levels for all the three groups show a decreasing trend, although nonsignificant, over the 30-day time period. The LPx levels in the kidney [Figure 3(b)] showed no statistically significant change with time for the three groups. At each time point,

no statistically significant difference was observed among the three groups, except at day 10. At day 10, Gd-SWCNTs showed higher LPx levels compared with the other two groups. The LPx levels in the spleen [Figure 3(c)] showed no statistically significant change with time for the PEG-DSPE and Fe-SWCNT groups. The LPx levels in Gd-SWCNT showed an increase with time. At each time point, there was no statistically significant difference in the LPx levels between the three groups. The results show no definite trend in the LPx levels in the lungs with time [Figure 3(d)] for the three groups. The LPx levels between the groups were statistically different at day 1 and day 30. The Gd-SWCNT group showed significantly increased LPx levels compared with the other two groups at day 1. PEG-DSPE showed higher LPx levels compared with Fe-SWCNTs and Gd-SWCNTs at day 30. Because the injected Fe-SWCNTs and Gd-SWCNTs circulate for few hours within the blood, the LPx levels in plasma was also measured. The results showed no significant changes in the plasma LPx levels with time or within the groups at each time point [Figure 3(e)]. Another molecular indicator of inflammation is the presence of proinflammatory cytokines such as TNF-α.[38] Therefore, plasma TNF-α levels were also analyzed at the four time points, and the results showed no significant changes with time for all groups (data not shown). Moreover, at each time point, no differences in the plasma TNF-α levels were observed between the groups.

The formation of LPx in the organs is an indication of oxidative stress–induced damage caused by the nanotubes. Oxidative stress–induced LPx formation is implicated in a variety of disorders.[39] The reason for the increased LPx levels at the lower time period could be due to the imbalance between the pro-oxidants (free radicals generated by inflammatory cells) and antioxidant defense systems, with predominantly pro-oxidant levels. The absence of LPx at later time points in the organs maybe due to the enhanced regulation of antioxidant defense system (not measured in the current study) to maintain organ homeostasis. These results are similar with a recent study with Fe-SWCNTs covalently functionalized with carboxylic acid groups and intraperitoneally injected at the same dose (0.5 mg/kg).[31]

Genome response

The effects of the three groups on the liver genes were evaluated using DNA microarray. Liver tissue was chosen for this analysis, because it is an important site for xenobiotic metabolism, and recent studies have indicated that nanotubes can get trapped by the RES after intravenous injections and retained mainly in the liver.[23,40] Only twofold alteration in genes regulation compared with PEG-DSPE (control 2) were considered significant and included in the analysis. Table II summarizes the salient results of global gene expression profiles (Supporting Information Table S2 lists the gene expression profiles) of the Gd-SWCNTs and Fe-SWCNT compared with PEG-DSPE. Overall, the microarray data indicate that the Gd-SWCNTs and Fe-SWCNTs differentially modulate hepatic gene expression. Of the total 33,000 genes analyzed, only 42 genes (~0.13%) in the Gd-SWCNT group showed at least twofold alteration compared with control 2; 21 known genes were upregulated, nine known genes were downregulated, and 12 genes were unknown or not yet characterized. Nine of these unknown genes were upregulated and three genes were downregulated. Multiple genes up or downregulated by the Gd-SWCNTs code for cell characteristics such as catalytic activity, nucleic acid and protein binding, transport proteins, transcription factors, nucleus, organelles, membranes (Supporting Information, Table S3a). A total of 15 genes (~0.04%) in the Fe-SWCNT group were altered compared with control 2; eight known genes were upregulated, two genes were downregulated, and five genes were yet to be characterized. Two of these unknown genes were upregulated, and three genes were downregulated (Supporting Information, Table S3b). The Fe-SWCNTs up or downregulated multiple genes for cellular characteristics such as transport proteins, nucleus, and organelles. The genes common to Gd-SWCNTs and Fe-SWCNTs (upregulated: Onecut1, Slc25a25,

Scd1, Sds; downregulated: Bcl6, Cxcl1) are involved in transport and transcriptional regulation (Table II). Majority of the up or downregulated genes for the Gd-SWCNTs and Fe-SWCNTs are located in the cell nucleus, cytoplasm, and cellular organelles. In both the groups, the Cxcl1 gene, which acts as a neutrophil chemoattractant or plays a role in the acute phase of the inflammatory response, was highly repressed. The table and its analysis shows that gene regulatory mechanisms involved in response to both these nanoparticles include the regulation of transport and transcriptional activity and downregulation of inflammatory response. In addition, the analysis suggests that the regulation of genes involved in catalytic activity mediate the transcriptional regulation of genes involved in suppressing the inflammatory gene or regulating the cellular/organ development and fatty acid metabolism. The results also show that the small but diverse gene regulation profile do not follow any specific cell signaling pathways, suggesting that the regulated genes are mainly involved in the physiological homeostasis. To the best of our knowledge, this is the first study that has characterized the *in vivo* genetic expression profiles of water-solubilized Gd-SWCNTs or Fe-SWCNTs. Although there have been no reports that have characterized the *in vitro* gene profiles of liver cells in the presence of Gd-SWCNTs or Fe-SWCNTs, a recent *in vitro* study has highlighted the various types of genes regulated in response to Fe-SWCNTs on human normal lung cells.[41] In that study, ~26% genes were regulated at a dosage of 0.1 mg/mL, which is considered a toxic dosage. That study focused on occupational health conditions where inhalation of nanotubes at toxic dosages is possible. However, for potential *in vivo* biomedical applications, nanotubes will be used at potentially nontoxic dosages, and it is important to evaluate their genetic effects at these dosages as well. Our results suggest that at potentially nontoxic dosages, the several lines of *in vivo* defense mechanisms (absent *in vitro* where typically one cell line is used) may prevent or mitigate large changes in the expression of gene expression profiles.

The results of this study indicate that the Gd-SWCNTs, water-solubilized with PEG-DSPE, injected intravenously at a potentially nontoxic dosage does not illicit any inflammatory response at the organ/ tissue and molecular level. Their response is similar to Fe-SWCNTs water-solubilized with PEG-DSPE or only PEG-DSPE. The results also show that the Gd-SWCNTs and Fe-SWCNTs have minor differential effects at the genomic level. However, these results cannot be extended to other SWCNT Gd^{3+} complexes[9–11] or SWCNT synthesized with other metal catalysts (e.g., cobalt or nickel),[16] which may have different pharmacodynamics behavior, because of significant differences in their synthesis methods, size, and chemical compositions. Although the pharmacodynamic results of the Gd-SWCNTs at potentially nontoxic dosages are promising, additional *in vivo* work is needed to investigate its vasoactivity in normal small animals[42] or whether it induced NSF in small animal renal disease models.[14] Nevertheless, this study opens avenues for further assessment of the imaging efficacy of Gd-SWCNTs by MRI. Previous phantom MRI of Gd-SWCNTs showed that their MRI signal intensity is 14 times greater than clinical Gd-based MRI CAs at 3 Tesla magnetic fields. Therefore, the Gd-SWCNTs should show contrast enhancement at low dosages. This study additionally presents possibility of further *in vivo* imaging studies with Fe-SWCNTs, which show potential as T_2 MRI CAs.[43]

CONCLUSIONS

In summary, the results of this study indicate that PEG-DSPE water-solubilized Gd-SWCNTs injected intravenously into rats at nontoxic dosages do not illicit an inflammatory response at the organ, tissue, and molecular level and that their response is similar to PEG-DSPE water-solubilized Fe-SWCNTs or DPSE-PEG only. The results show that both Gd-SWCNTs and Fe-SWCNTs marginally increase proinflammatory lipid peroxide levels 24 h postinjection in liver and lungs, which decreases with time. The nanotubes get out of the circulatory system within 24 h, accumulate within different organs (lungs, brain, kidney,

liver, and spleen) for few days, and are eliminated from the body within 10 days. The results also show that the Gd-SWCNT and Fe-SWCNT have minor and differential effect at the genomic level mainly to maintain liver homeostasis.

Supplementary Material

Refer to Web version on PubMed Central for supplementary material.

Acknowledgments

The authors thank Dr. John Schwedes and Dr. Jizu Zhi for DNA Microarray and Bioinformatics analysis. The authors also thank Stephanie Burke and Mallory Korman for their help with immunostaining, Susan Van Horn for transmission electron microscope image acquisition, and Gaurav Lalwani for editorial help.

Contract grant sponsor: Breast Cancer Research Program of the Department of Defense; contract grant number: W81XWH-10-1-0521.

Contract grant sponsor: Carol M. Baldwin Fund

REFERENCES

1. Mansfield P. Snapshot magnetic resonance imaging (Nobel lecture). Angew Chem Int Ed Engl. 2004; 43:5456–5464. [PubMed: 15384128]
2. Merbach, AE.; Toth, E. The Chemistry of Contrast Agents in Medical Magnetic Resonance Imaging. Chichester, New York: Wiley; 2001.
3. Aime S, Botta M, Terreno E. Gd(III)-based contrast agents for MRI. Adv Inorg Chem. 2005; 57:173–237.
4. Caravan P, Ellison JJ, McMurry TJ, Lauffer RB. Gadolinium(III) chelates as MRI contrast agents: Structure, dynamics, and applications. Chem Rev. 1999; 99:2293–2352. [PubMed: 11749483]
5. Na HB, Hyeon T. Nanostructured T1 MRI contrast agents. J Mater Chem. 2009; 19:6267–6273.
6. Nunn AD, Linder KE, Tweedle MF. Can receptors be imaged with MRI agents? Q J Nucl Med. 1997; 41:155–162. [PubMed: 9203854]
7. Sitharaman B, Wilson LJ. Gadonanotubes as new high-performance MRI contrast agents. Int J Nanomedicine. 2006; 1:291–295. [PubMed: 17717970]
8. Sitharaman B, Tran LA, Pham QP, Bolskar RD, Muthupillai R, Flamm SD, Mikos AG, Wilson LJ. Gadofullerenes as nanoscale magnetic labels for cellular MRI. Contrast Media Mol Imaging. 2007; 2:139–146. [PubMed: 17583898]
9. Richard C, Doan BT, Beloeil JC, Bessodes M, Tóth & Eacute, Scherman D. Noncovalent functionalization of carbon nanotubes with amphiphilic Gd3+ chelates: Toward powerful T1 and T2 MRI contrast agents. Nano Lett. 2008; 8:232–236. [PubMed: 18088153]
10. Tran LA, Krishnamurthy R, Muthupillai R, Cabreira-Hansen MD, Willerson JT, Perin EC, Wilson LJ. Gadonanotubes as magnetic nanolabels for stem cell detection. Biomaterials. 2010; 31:9482–9491. [PubMed: 20965562]
11. Hassan AA, Chan BTY, Tran LA, Hartman KB, Ananta JS, Mackeyev Y, Hu LY, Pautler RG, Wilson LJ, Lee AV. Serine-derivatized gadonanotubes as magnetic nanoprobes for intracellular labeling. Contrast Media Mol Imaging. 2010; 5:34–38. [PubMed: 20101755]
12. Sitharaman B, Zande MVD, Ananta JS, Shi X, Veltien A, Walboomers XF, Wilson LJ, Mikos AG, Heerschap A, Jansen JA. Magnetic resonance imaging studies on gadonanotube-reinforced biodegradable polymer nanocomposites. J Biomed Mater Res Part A. 2010; 93A:1454–1462.
13. Zande MVD, Sitharaman B, Walboomers XF, Tran L, Ananta JS, Veltien A, Wilson LJ, Álava JI, Heerschap A, Mikos AG, Jansen JA. In vivo magnetic resonance imaging of the distribution pattern of gadonanotubes released from a degrading poly(lactic-co-glycolic acid) scaffold. Tissue Eng Part C: Methods. 2011; 17:19–26.

14. Idee JM, Port M, Medina C, Lancelot E, Fayoux E, Ballet S, Corot C. Possible involvement of gadolinium chelates in the pathophysiology of nephrogenic systemic fibrosis: A critical review. Toxicology. 2008; 248:77–88. [PubMed: 18440117]
15. FDA Drug Safety Communication: New warnings for using gadolinium-based contrast agents in patients with kidney dysfunction. Drug Safety and Availability: FDA U.S. Food and Drug Administration. 2010
16. Liu Z, Tabakman S, Welsher K, Dai H. Carbon nanotubes in biology and medicine: In vitro and in vivo detection, imaging and drug delivery. Nano Res. 2009; 2:85–120. [PubMed: 20174481]
17. Swierczewska M, Rusakova I, Sitharaman B. Gadolinium and europium catalyzed growth of single-walled carbon nanotubes. Carbon. 2009; 47:3139–3142.
18. Sitharaman B, Rajamani S, Avti PK. Time-resolved red luminescence from europium-catalyzed single walled carbon nanotubes. Chem Commun. 2011; 47:1607–1609.
19. Sitharaman B, Jacobson B, Wadghiri YZ, Bryant H, Frank J. The magnetic, relaxometric and optical properties of gadolinium-catalyzed single walled carbon nanotubes. J Appl Phys; Forthcoming.
20. Avti PK, Caparelli DE, Sitharaman B. Cytotoxicity, cytocompatibility, cell-labeling efficiencies, and in vitro cellular magnetic resonance imaging of gadolinium-catalyzed single-walled carbon nanotubes. J Biomed Mater Res Part A; Forthcoming.
21. Liu Z, Davis C, Cai W, He L, Chen X, Dai H. Circulation and long-term fate of functionalized, biocompatible single-walled carbon nanotubes in mice probed by Raman spectroscopy. Proc Natl Acad Sci USA. 2008; 105:1410–1415. [PubMed: 18230737]
22. Hendriks T, Assmann RF. On the fluorometric assay of circulating lipoperoxides. Clin Chim Acta. 1988; 174:263–269. [PubMed: 3134146]
23. Liu Z, Cai W, He L, Nakayama N, Chen K, Sun X, Dai H. In vivo biodistribution and highly efficient tumour targeting of carbon nanotubes in mice. Nat Nanotechnol. 2007; 2:47–52. [PubMed: 18654207]
24. Malle E, Furtmuller PG, Sattler W, Obinger C. Myeloperoxidase: A target for new drug development? Br J Pharmacol. 2007; 152:838–854. [PubMed: 17592500]
25. Gupta RB, Harpaz N, Itzkowitz S, Hossain S, Matula S, Kornbluth A, Bodian C, Ullman T. Histologic inflammation is a risk factor for progression to colorectal neoplasia in ulcerative colitis: A cohort study. Gastroenterology. 2007; 133:1099–1105. [PubMed: 17919486]
26. Kagan VE, Konduru NV, Feng W, Allen BL, Conroy J, Volkov Y, Vlasova II, Belikova NA, Yanamala N, Kapralov A, et al. Carbon nanotubes degraded by neutrophil myeloperoxidase induce less pulmonary inflammation. Nat Nanotechnol. 2010; 5:354–359. [PubMed: 20364135]
27. Shvedova AA, Kapralov AA, Feng WH, Kisin ER, Murray AR, Mercer RR, St Croix CM, Lang MA, Watkins SC, Konduru NV, et al. Impaired clearance and enhanced pulmonary inflammatory/fibrotic response to carbon nanotubes in myeloperoxidase-deficient mice. PLoS One. 2012; 7:e30923. [PubMed: 22479306]
28. Kapralov AA, Feng WH, Amoscato AA, Yanamala N, Balasubramanian K, Winnica DE, Kisin ER, Kotchey GP, Gou PP, Sparvero LJ, et al. Adsorption of surfactant lipids by single-walled carbon nanotubes in mouse lung upon pharyngeal aspiration. ACS Nano. 2012; 6:4147–4156. [PubMed: 22463369]
29. Lam CW, James JT, McCluskey R, Hunter RL. Pulmonary toxicity of single-wall carbon nanotubes in mice 7 and 90 days after intra-tracheal instillation. Toxicol Sci. 2004; 77:126–134. [PubMed: 14514958]
30. Warheit DB, Laurence BR, Reed KL, Roach DH, Reynolds GA, Webb TR. Comparative pulmonary toxicity assessment of single-wall carbon nanotubes in rats. Toxicol Sci. 2004; 77:117–125. [PubMed: 14514968]
31. Patlolla A, McGinnis B, Tchounwou P. Biochemical and histopathological evaluation of functionalized single-walled carbon nanotubes in Swiss-Webster mice. J Appl Toxicol. 2011; 31:75–83. [PubMed: 20737426]
32. Lee HJ, Park J, Yoon OJ, Kim HW, Lee do Y, Kim do H, Lee WB, Lee NE, Bonventre JV, Kim SS. Amine-modified single-walled carbon nanotubes protect neurons from injury in a rat stroke model. Nat Nanotechnol. 2011; 6:121–125. [PubMed: 21278749]

33. McDevitt MR, Chattopadhyay D, Kappel BJ, Jaggi JS, Schiffman SR, Antczak C, Njardarson JT, Brentjens R, Scheinberg DA. Tumor targeting with antibody-functionalized, radiolabeled carbon nanotubes. J Nucl Med. 2007; 48:1180–1189. [PubMed: 17607040]
34. Singh R, Pantarotto D, Lacerda L, Pastorin G, Klumpp C, Prato M, Bianco A, Kostarelos K. Tissue biodistribution and blood clearance rates of intravenously administered carbon nanotube radiotracers. Proc Natl Acad Sci USA. 2006; 103:3357–3362. [PubMed: 16492781]
35. Cherukuri P, Gannon CJ, Leeuw TK, Schmidt HK, Smalley RE, Curley SA, Weisman RB. Mammalian pharmacokinetics of carbon nanotubes using intrinsic near-infrared fluorescence. Proc Natl Acad Sci USA. 2006; 103:18882–18886. [PubMed: 17135351]
36. Yang ST, Wang X, Jia G, Gu Y, Wang T, Nie H, Ge C, Wang H, Liu Y. Long-term accumulation and low toxicity of single-walled carbon nanotubes in intravenously exposed mice. Toxicol Lett. 2008; 181:182–189. [PubMed: 18760340]
37. Yang S-T, Guo W, Lin Y, Deng X-Y, Wang H-F, Sun H-F, Liu Y-F, Wang X, Wang W, Chen M, et al. Biodistribution of pristine single-walled carbon nanotubes in vivo. J Phys Chem C. 2007; 111:17761–17764.
38. Laskin DL, Pendino KJ. Macrophages and inflammatory mediators in tissue injury. Annu Rev Pharmacol Toxicol. 1995; 35:655–677. [PubMed: 7598511]
39. Alvarez-Gonzalez R. Free radicals, oxidative stress, and DNA metabolism in human cancer. Cancer Invest. 1999; 17:376–377. [PubMed: 10370368]
40. Deng X, Yang S, Nie H, Wang H, Liu Y. A generally adoptable radiotracing method for tracking carbon nanotubes in animals. Nanotechnology. 2008; 19:75–101.
41. Alazzam A, Mfoumou E, Stiharu I, Kassab A, Darnel A, Yasmeen A, Sivakumar N, Bhat R, Al Moustafa AE. Identification of deregulated genes by single wall carbon-nanotubes in human normal bronchial epithelial cells. Nanomedicine. 2010; 6:563–569. [PubMed: 20060075]
42. Rivers RJ, Beckman JB, Frame MD. Technique for using video-microscopy and indicator dilution for repeated measurements of cardiac output in small animals. Anesthesiology. 2001; 94:489–495. [PubMed: 11374611]
43. Choi JH, Nguyen FT, Barone PW, Heller DA, Moll AE, Patel D, Boppart SA, Strano MS. Multimodal biomedical imaging with asymmetric single-walled carbon nanotube/iron oxide nanoparticle complexes. Nano Lett. 2007; 7:861–867. [PubMed: 17335265]

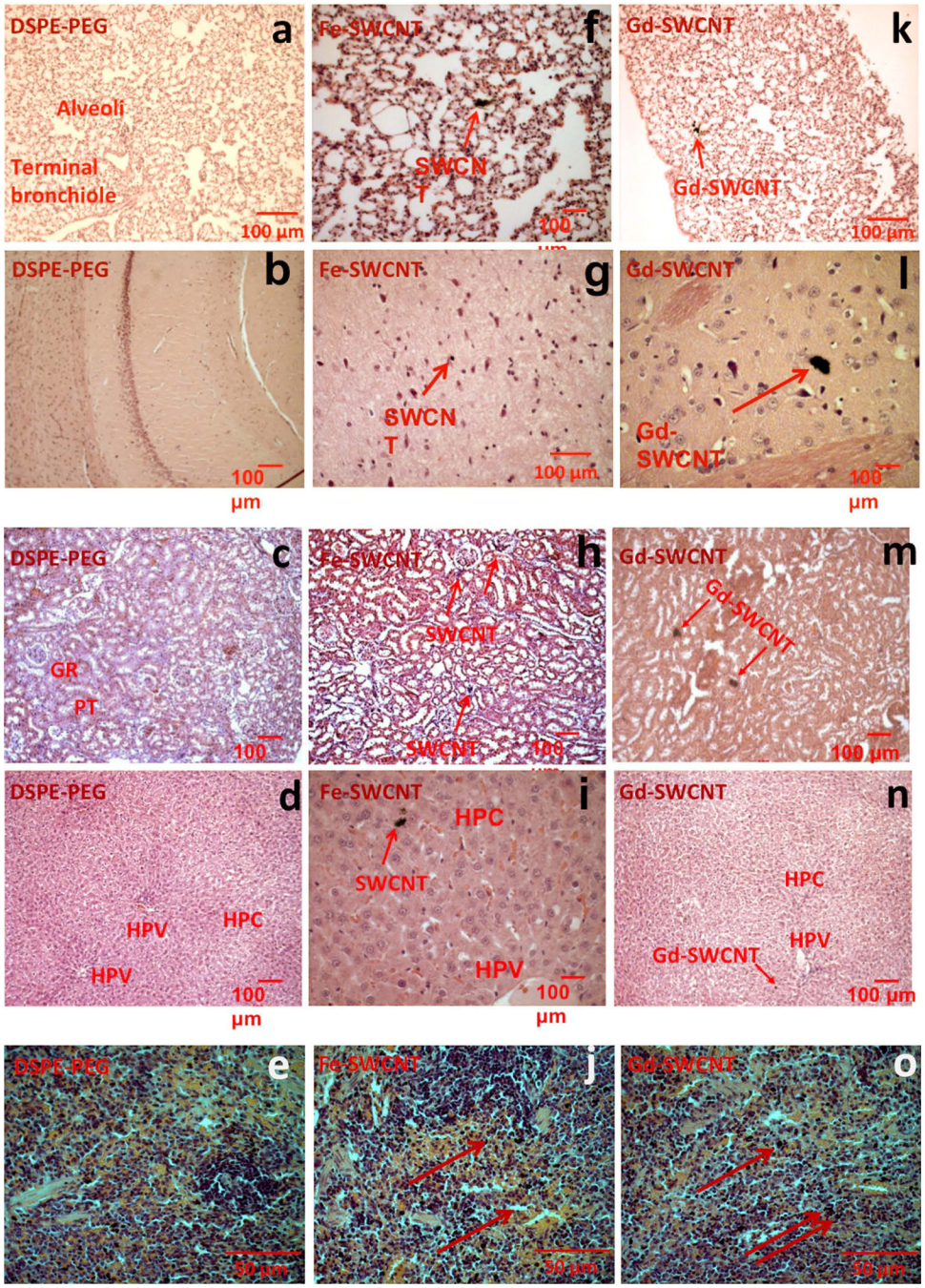

FIGURE 1.

Representative histological specimens (H&E staining) at day 1 of rat (a, f, k) lung (b, g, l), brain (c, h, m), kidney (d, i, n), liver, and (e, j, o) spleen for PEG-DSPE, Fe-SWCNTs treatment, and Gd-SWCNT. Gd-SWCNT and Fe-SWCNT aggregates (red arrows) are found in lungs, brain, kidney, liver, and spleen. Gd-SWCNT aggregates are also found in lungs, brain, kidney, liver, and spleen. The Gd-SWCNTs and Fe-SWCNT are aggregated in the alveolar epithelial lining of the lungs (f and k), in the cerebral cortex of brain (g and l), in the proximal tubules of the kidney (h and m), in the hepatocytes of liver (i and n), and in the red pulp of spleen (j and o). The histological specimens do not show any signs of inflammation

or tissue architectural damage. [Color figure can be viewed in the online issue, which is available at www.interscience.wiley.com.]

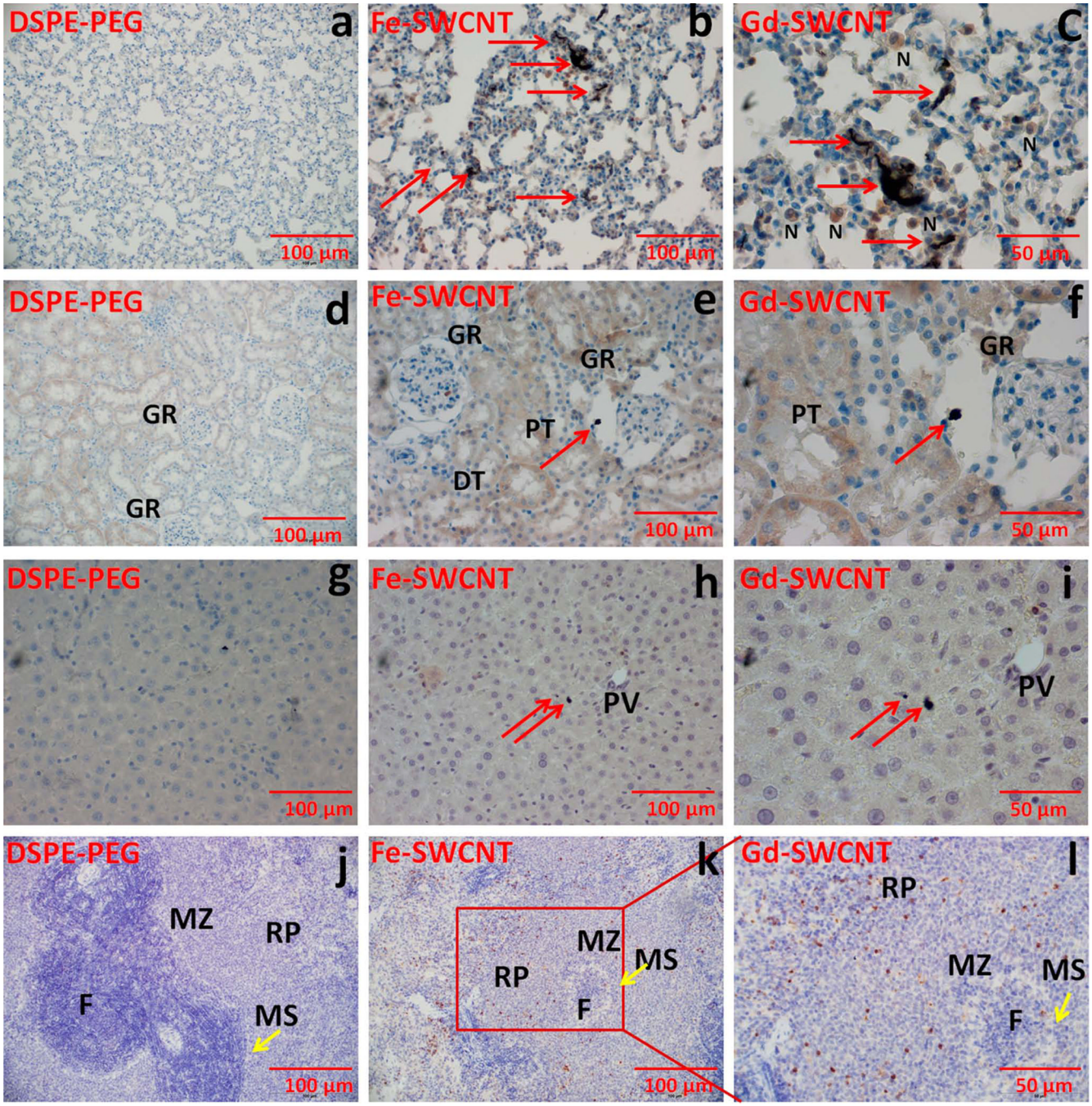

FIGURE 2.

Representative myeloperoxidase (MPO) immunostained specimens at day 1 of rat (a, b, c) lung (d, e, f), kidney (g, h, i), liver, and (j, k, l) spleen for PEG-DSPE, Fe-SWCNTs treatment, and Gd-SWCNT. Gd-SWCNT aggregates (red arrows) are found in lungs (b, c), kidney (e, f), liver (h, i), and spleen (k, l). The Gd-SWCNTs are aggregated in the alveolar epithelial lining of the lungs with few neutrophils (N) surrounding the Gd-SWCNTs; in the kidney glomerulus (GR) and in the hepatocytes of liver. The specimens do not show any signs of inflammation or tissue architectural damage. There were no changes in the MPO expression in lungs, kidney, liver, and spleen. GR, glomerulus; PT, proximal tubule; DT, distal tubule; PV, hepatic portal vein; F, follicle; MZ, marginal zone; MS, marginal sinus.

[Color figure can be viewed in the online issue, which is available at www.interscience.wiley.com.]

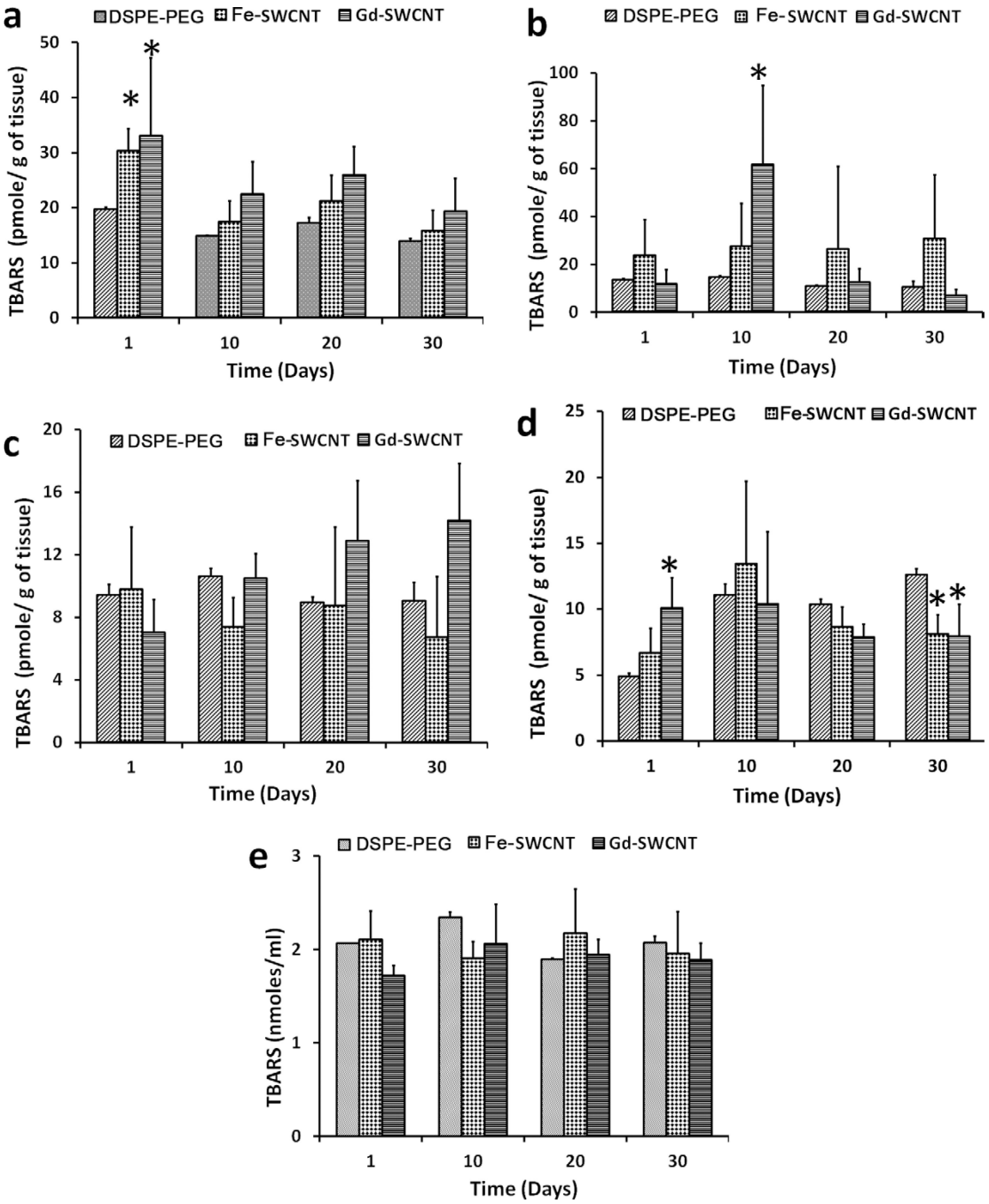

FIGURE 3.

Lipid peroxidation levels for DSPE PEG, Fe-SWCNT, and Gd-SWCNT group in the (a) liver, (b) kidney, (c) spleen, (d) lungs, and (e) plasma at day 1, 10, 20, and 30 postinjection. Data are presented as mean ± standard deviation ($n = 5$; * indicates $p < 0.05$ between groups at that time point).

TABLE I

Scoring of Myeloperoxidase Immunostained Neutrophils in Various Organs

Groups[a]	Average Number of Cells Per Field
$Lu_{Fe\text{-}SWCNT}$	15.5
$Lu_{Gd\text{-}SWCNT}$	10
$Li_{Fe\text{-}SWCNT}$	17.1
$Li_{Gd\text{-}SWCNT}$	18.4
$K_{Fe\text{-}SWCNT}$	0.7
$K_{Gd\text{-}SWCNT}$	0.5
$B_{Fe\text{-}SWCNT}$	0.2
$B_{Gd\text{-}SWCNT}$	0.1
$S_{Fe\text{-}SWCNT}$	1.8
$S_{Gd\text{-}SWCNT}$	0

For each slide, 10 field views were randomly selected and counted for the immunostained neutrophils in various organs.

[a]Lu, lungs; Li, liver; K, kidney; B, brain; S, spleen.

TABLE II

Liver Genes at Day 1 Showing At Least Twofold ($p < 0.05$) Change in Regulation for Gd-SWCNTs or Fe-SWCNTs Compared With PEG-DSPE

		Upregulated Genes		Downregulated Genes	
No.	**Cell Characteristics**	**Gd-SWCNT**	**Fe-SWCNT**	**Gd-SWCNT**	**Fe-SWCNT**
		Cell function			
1	Catalytic activity	Sds, Scd1, Usp2, Elovl6, Prss32	Sds	Cyp2b1/Cyp2b2	—
2	Nucleic acid binding	Zfp354a, Zfp37, Onecut1, Dbp	Onecut1	Egr1, Arnt1, Bcl6, Rora	Bcl6
3	Protein binding	Prkcdbp, Fasn, Ifrd1, Per2	—	Pnrc1, Efna1	—
4	Protein degradation	Prss32	—	—	—
5	Protein transport	Slc2a5, Slc25a25, Mfsd2, Bcl6	Slc25a25, Slc25a30	Slc6a6, Arntl	—
6	Inflammatory response	—	—	Cxcl1	Cscl1
7	Liver development	Onecut1	Onecut1	—	—
8	Cellular/organ development	Ifrd1, Ky	—	—	—
9	Cellular signaling	—	—	Efna1	—
10	Cell growth regulation	Prkcdbp,	—	Osgin1	—
11	Gluconeogenesis	Sds	Sds	—	—
12	Lipid metabolism	Scd1	Scd1	—	—
13	Fatty acid biosynthesis	Fasn, Elovl6,	—	—	—
14	Transcription	Per2, Zfp354a, Zfp37, Usp2, Dbp	Trib3	Egr1, Pnrc1, Rora	—
		Location in the cell of known regulated genes from the above list			
1	Nucleus	Ifrd1, Per2, Dbp, Zfp354a, Zfp37, Onecut1, Usp2,	Trib3, Onecut1	Egr1, Pnrc1, Arnt1, Bcl6, Rora	—
2	Cytoplasm	Fasn, Ifrd1, Per2, Sds, Usp2	Sds	Egr1,	—
3	Organelles	Fasn, Scd1, Slc25a25, Coq10b, Elov16	Scd1, Slc25a25, Slc25a30	Cyp2b1/Cyp2b2,	Bcl6
4	Membrane	Ifrd1, Slc2a5, Slc25a25, Prss32	—	Slc6a6, Efna1	—
5	Extracellular	—	—	Cxcl1	Cxcl1